Optical Fiber Technology 45 (2018) 295–299

Contents lists available at ScienceDirect

Optical Fiber Technology

journal homepage: www.elsevier.com/locate/yofte

Experimentally and analytically derived generalized model for the detection of liquids with suspended-core optical fibers

Tomas Nemecek[a,*], Matej Komanec[a], Bryan Nelsen[b,c], Tomas Martan[a], Dmytro Suslov[a], Peter Hartmann[b,c], Stanislav Zvanovec[a]

[a] Department of Electromagnetic Field, Faculty of Electrical Engineering, Czech Technical University in Prague, Technicka 2, Prague 6 166 27, Czech Republic
[b] Fraunhofer-Institut für Werkstoff- und Strahltechnik IWS, 01277 Dresden, Germany
[c] Institute of Leupold-Institute for Applied Natural Sciences/Optical Technologies, University of Applied Sciences Zwickau, 08056 Zwickau, Germany

ARTICLE INFO

Keywords:
Sensors
Fiber optics systems
Microstructured fibers
Refractometry

ABSTRACT

A generalized model for the detection of liquids within suspended-core microstructured optical fibers has been experimentally and theoretically derived. The sensor detection is based on the refractometric principle of transmission losses due to the overlap of the evanescent field with the liquid analyte. A number of parameters, including fiber core diameter and filling length, have been included in the general model. Specially tailored suspended-core fibers were manufactured with the core diameters within the range of 2.4 μm to 4.0 μm. Five selected liquid analytes were used to cover the refractive index range of 1.35 to 1.42. Based on experiments, the characteristics of the parameters of the semi-empirical model have been determined by a genetic algorithm using 283 measurement data sets. The model can be used to design sensors for the detection of liquid analytes as it provides a set of parameters allowing to optimize the sensor's sensitivity for a wide scale of applications. Finally, numerical simulations of the system were carried out by an eigenmode routine to support the results of the generalized model.

1. Introduction

Remote monitoring of the quality of liquids in toxic, explosive or flammable environments is essential for safety and is required in various industrial and agricultural processes. Fiber-optic sensors provide many advantages over electronic sensors, including their small size and low weight, their immunity to electromagnetic interference, the absence of any sparks, their long lifetime and easy system integration.

To enhance fiber-optic sensor features, especially sensitivity and resolution, special optical fiber designs have been developed employing microstructured optical fibers (MOFs) [1,2]. The potential of MOFs for optical detection lies in the possibility of tailoring the MOF structure to achieve enhanced sensor performance [3]. Among MOFs, suspended-core MOFs (SC-MOFs) can provide significantly increased evanescent field overlap with the measured analyte, making them exceptionally suitable for the purposes of the detection of liquid analytes. An overview of SC-MOF sensor applications is summarized in [4,5]. SC-MOF sensors focusing on specific liquid analytes or in-liquid particles were developed using plasmon resonance [6,7] and other spectroscopic sensing methods [8]. Even though the abovementioned SC-MOF sensors provide high sensitivity, they require a complex multi-step sensor preparation, often including opto-chemical transducers.

Refractive index-based sensors represent a simplified and universal sensor approach for the detection of liquid analytes, e.g. in petrol quality analysis, where the refractive index of gasoline change as a result of blending with bioalcohol was studied in [9] and similarly ethanol-gasoline concentration was measured by long-period gratings in [10]. Several SC-MOF structural modifications for the detection of liquid analytes have been previously presented as an exposed-core fiber [11,12]. Conventional and selective hole filling of SC-MOF was also examined [13,14]. The combination of fiber Bragg gratings and SC-MOF was presented in [15], where the achieved sensitivity was up to 100 nm/RIU. Resonance based RI sensing was demonstrated by MOF tapering, resulting in air-hole collapse [16], where the resolution acquired by this approach was around 1×10^{-5} RIU. An interference-based sensor, consisting of two air-clad MOFs spliced between standard single-mode fibers, was presented in [17], indicated sensitivity was 230 nm/RIU and achieving resolution of 3.4×10^{-5} RIU.

This paper significantly extends our previous work [18] by developing an analytical description of optical signal propagation within a liquid analyte filled SC-MOF. Based on an extensive amount of experimental data, a generalized model is derived, which describes the

* Corresponding author.
E-mail address: nemect10@fel.cvut.cz (T. Nemecek).

https://doi.org/10.1016/j.yofte.2018.08.005
Received 25 May 2018; Received in revised form 18 July 2018; Accepted 3 August 2018

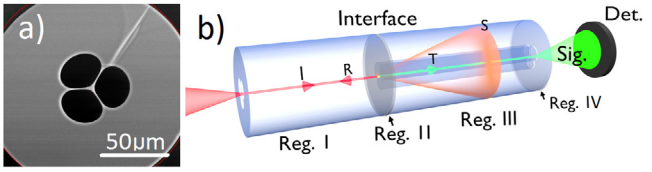

Fig. 1. a) Scanning-electron microscope (SEM) image of the end-face of a 4 μm core diameter SC-MOF and b) a schematic representation the studied interactions inside the SC-MOF studied; Det – Detector, Sig – Signal, I – Incident, R – Reflected, T – Transmitted and S – Scattered light. Region I – air-filled cladding holes, Region II – air-clad liquid-clad interface, Region III – liquid-filled cladding holes, Region IV – liquid-filled cladding free-space interface.

theoretical and empirical behavior of the SC-MOF sensor. This model can be used as a universal tool for SC-MOF sensor design.

2. Light propagation in SC-MOF structure

The mechanisms which cause losses in a partially liquid-filled SC-MOF (shown in Fig. 1) can be divided into two essential loss contributions. The major loss sources are illustrated in Fig. 1 b). The first of them is represented by reflection and scattering losses at the boundary where the air-filled cladding (depicted as Region I) interfaces the liquid-filled cladding (depicted as Region II), as well as in the case of the interface of liquid-filled cladding (depicted as Region III) and free-space at the end of the SC-MOF (depicted as Region IV). Region IV further represents radiation from the SC-MOF end-face. The second type of loss is caused by the evanescent component of the SC-MOF mode being either absorbed or scattered by the liquid analyte itself (Region III).

A numerical-based solution of the losses in the liquid-filled SC-MOF was carried out by a self-developed eigenmode routine using a finite-difference method with a sparse-matrix eigenvalue solver which we utilized to solve the propagation of modes in both the air- and liquid-filled sections of the SC-MOF sensor (Region I and Region III). It was important to consider the full-polarization form of the wave equation because the tight confinement of the modes depends strongly on the boundary conditions between glass and air, or, glass and the liquid analyte (previously defined in [18]). A set of first-order polarized guided modes derived for SC-MOF, with a core diameter (d_{core}) of 4 μm, is shown in Fig. 2.

It was assumed, for the purpose of simplicity, that only the fundamental mode is excited in Region I. The model can be written as:

$$\overrightarrow{E_{III}} = a_0 \overrightarrow{E_O} + \overrightarrow{E_s}, \tag{1}$$

where $\overrightarrow{E_s}$ is light scattered at the interface, $\overrightarrow{E_0}$ is the normalized fundamental mode electric field in Region III and $|a_0|^2$ gives the fraction of power coupled into the outgoing fundamental mode [19], used as the input field for Region III. It is assumed that the remaining power $(1-|a_0|^2)$ is scattered into the cladding modes and mostly lost due to scattering out of SC-MOF. The power, therefore, transferred to the fundamental mode of Region III at the interface (Region II) is given by:

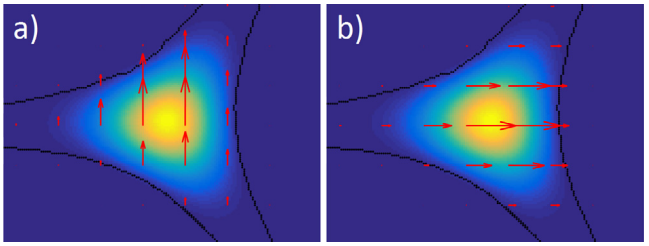

Fig. 2. Numerically calculated polarized fundamental modes of the SC-MOF with a 4 μm core diameter at 1550 nm. a) and b) are orthogonal to each other, $\beta = 5.788\,\mu m^{-1}$.

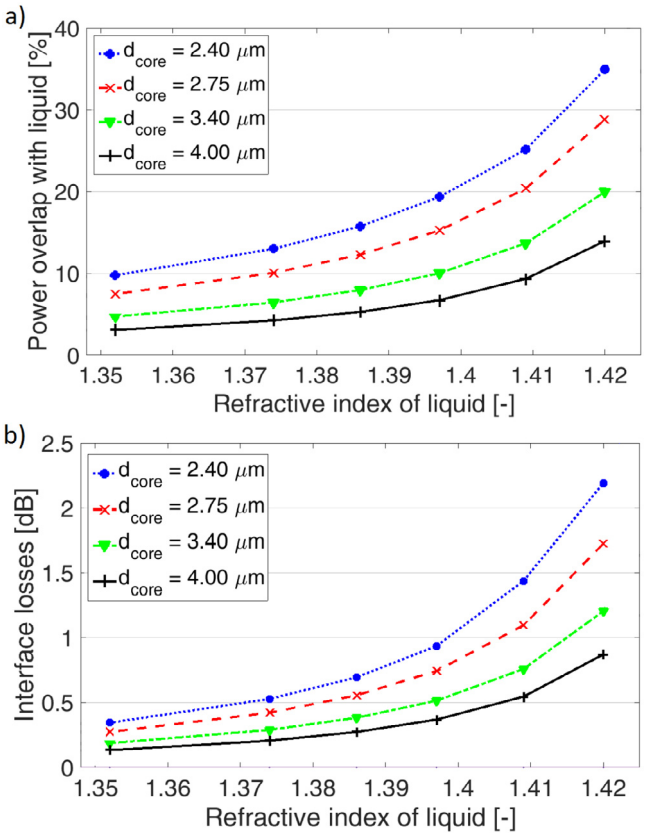

Fig. 3. Finite difference results of a) the power overlap with liquid analytes with respect to SC-MOF core diameters for Region III (see Eq. (1)) and b) losses due to reflection and scattering at the interface (Eq. (2)).

$$P_{III} = |a_0|^2 P_I, \tag{2}$$

with P_I, P_{III} being the power in Regions I and III, respectively (reflection at this interface was calculated to be extremely small because the mode in Region I is very tightly confined in the glass core of the SC-MOF). Once the light has entered Region III, the liquid analyte gives rise to both absorption losses and weak scattering losses. Both loss coefficients are proportional to the distance traveled through the liquid analyte and the power overlap of the fundamental mode with the liquid analyte. The differential power loss in Region III can be expressed as:

$$\frac{\partial P}{\partial z} = -(\rho_a \sigma_{abs} + \rho_s \sigma_{scatt})\eta P, \tag{3}$$

where P is the power along the length of SC-MOF, σ_{abs}, σ_{scatt} are the absorption and scattering cross-sections, respectively, ρ_a and ρ_s are the density of absorbing and scattering centers in the liquid analyte, respectively, and η is the percentage of mode intensity overlap with the liquid analyte. The derived dependencies of power overlapping with liquid and interface losses on RI and core diameter are shown in Fig. 3. The solution to Eq. (3), considering the full length of the liquid-filled section, can be written as:

$$P = P_{III} e^{-(\rho_a \sigma_{abs} + \rho_s \sigma_{scatt})\eta l_{fill}}, \tag{4}$$

where l_{fill} is the length of liquid-filled SC-MOF, and P_{III} stands for the power at the input interface of Region III.

The losses in Region IV do not change significantly from the completely unfilled SC-MOF to the filled case. Since the losses of the filled SC-MOF will be calculated relative to that of the completely unfilled SC-MOF, losses due to Region IV are not included in the final equation.

Finally, inserting Eq. (2) into Eq. (4), the attenuation caused by liquid analyte in the SC-MOF sensor can be determined in [dB] by: